Biochimica et Biophysica Acta, 1148 (1993) 139–151

BBAMEM 75941

Fluorescence anisotropy studies on the interaction of the short chain n-alkanols with stratum corneum lipid liposomes (SCLL) and distearoylphosphatidylcholine (DSPC)/distearoylphosphatidic acid (DSPA) liposomes

Yong-Hee Kim [a], William I. Higuchi [a], James N. Herron [a] and William Abraham [b,1]

[a] *Department of Pharmaceutics, University of Utah, Salt Lake City, UT (USA) and* [b] *Department of Dermatology, University of Iowa, Iowa City, IA (USA)*

(Received 28 December 1992)

Key words: Short chain n-alkanol; Enhancement factor; Fluidity; Fluorescence anisotropy; Fluorescence lifetime; Stratum corneum lipid liposome

Previously, the action of the short chain n-alkanols (from C1 to C5) and isopropanol as possible enhancers on the transport of lipophilic and polar/ionic permeants across hairless mouse skin was investigated [1–4]. In the present study, the steady-state fluorescence anisotropy was measured as a means of estimating the changes in fluidity caused by the n-alkanols at different depths in the stratum corneum lipid liposomes (SCLL). Some selected experiments with the distearoylphosphatidylcholine (DSPC)/distearoylphosphatidic acid (DSPA) liposomes were performed for relative comparisons. The effects of the n-alkanols on polarity sensitive parameters such as fluorescence lifetimes, fluorescence quantum yield ratios, and emission maxima were studied in the SCLL. The polarity of the bilayer decreased as the fluorescent probe was placed closer to the bilayer center and the n-alkanols did not alter this gradient. Assessment of the depth-dependent effects of the n-alkanols using SCLL showed that most of the significant changes in fluidity induced by the n-alkanols were observed at intermediate depths (C2–C9) and there was little or no increase in fluidity in the deep hydrophobic region close to the bilayer center. These results suggest that the short chain n-alkanols work as effective 'fluidizing' agents at the intermediate depths (C2–C9) in the bilayer.

Introduction

The stratum corneum of skin has been considered a major barrier to the percutaneous absorption of drugs. Overcoming this barrier resistance by using transport enhancers has been one of the great interests in pharmaceutical research.

Recently, the influences of short chain n-alkanols (from C1 to C5) and isopropanol on the transport of lipophilic and polar/ionic permeants across hairless mouse skin were investigated [1–4]. A theoretical model was developed and the transport enhancement factor, E, for the lipoidal pathway of the stratum corneum was calculated from transport experiments at low levels of the alkanols present in saline. An E value of around 10 was found for lipophilic drugs at 30% ethanol, 10% n-propanol, 2% n-butanol, and 1% n-pentanol. Also, pretreatment studies showed that the effects of the n-alkanols at these concentrations were reversible as far as the lipoidal pathway of the stratum corneum was concerned.

A possible mechanism for the actions of the n-alkanols as transport enhancers was proposed: the enhancement effects may be related to the increases in fluidity in the appropriate transport rate-limiting lipid domain(s) [1–4]. Recent FTIR studies on the effects of short chain n-alkanols on the lipid alkyl chain packing, mobility, and conformational order at 37°C in hairless mouse stratum corneum and phospholipid liposomes [5,6] have indicated little or no increased fluidity of the hydrocarbon regions of the stratum corneum bilayers. From this, it was hypothesized that it may not be appropriate to consider the average of the hydrocarbon regions of the bilayer to represent the transport barrier and that some specific region such as the semi-polar interface of the intercellular lipid bilayers or the ordered hydrocarbon region near the interface may be viewed as the possible rate-limiting microenvironment of the lipoidal pathway.

Correspondence to: W.I. Higuchi, Department of Pharmaceutics, University of Utah, Salt Lake City, UT 84112, USA.

[1] Present address: Cygnus Therapeutic Systems, Redwood City, CA, USA.

In the present study, fluorescence anisotropy experiments with liposomes, including stratum corneum lipid liposomes, were conducted to examine changes in fluidity caused by the n-alkanols in lipid bilayers. The general term 'membrane fluidity' encompasses (1) orientational order of the acyl chains either collectively or as segments, (2) rotational diffusion of the same entities, and (3) translational diffusion [7]. From fluorescence anisotropy measurements we may infer both the orientational constraint (static or structural component) and restriction to the depolarizing rotational motions (dynamic or kinetic component) of the probe in a lipid bilayer by deducing from existing models estimates of the order parameter (S) and the rotational correlation time (ϕ), respectively [8–11].

Several recent publications have demonstrated that the early work on the determination of microviscosities from steady-state anisotropy (r_{ss}) measurements assuming isotropic rotation of a probe may be inappropriate since membrane bound fluorophores may exhibit anisotropic or hindered rotations. In the case of hindered rotation, the limiting anisotropy (r_∞) at long times after excitation does not return to zero because the fluorescent probe cannot rotate by 90° away from its original orientation [12–15]. The steady-state anisotropy, r_{ss}, may thus be frequently resolved into a 'static' component, r_∞, which is proportional to the square of the order parameter, and a 'dynamic' component, r_f. The quantity r_f may be related to the rotational correlation time which is proportional to the microviscosity [10,16,17]. Therefore, in lipid bilayers, r_{ss} may be described in terms of consequences of different rotational motions and constraints depending on which probe is used [8]. Rod-like linear probes like DPH (diphenylhexatriene) may exhibit a wobbling motion confined to a double hard-cone. This motion is sensitive to the packing density of the lipids and is related to the order parameter ($S = (r_\infty/r_0)^{0.5}$, where r_0 is the maximum anisotropy). On the other hand, planar, disc shaped probes such as anthracene attached to the fatty acids (anthroyloxy fatty acids, n-AF) can rotate by 90° around the C-O bond that attaches the anthroyloxy group to the fatty acid. In this case, the steady-state anisotropy is related to the rotational correlation time of the anthroyloxy group in the bilayer and reflects the microviscosity of the probe's local environment.

The interpretations of steady-state anisotropy data for DPH and n-AF have been discussed in detail in the literature [16–18] and two empirical relationships based on the theory of rotation dynamics in liquid crystals have been developed, which relate the steady-state anisotropy to the order parameter (S). Furthermore, Van der Meer et al. have modified the Perrin equation to include hindered rotation in lipid bilayers [17]. Both the empirical relationships and the modified Perrin equation have been used to describe the rotational dynamics of DPH and n-AF in a number of model lipid bilayers and naturally-occurring biomembranes [8,16–18].

In this study, we used two model lipid bilayers, distearoylphosphatidylcholine (DSPC)/distearoylphosphatidic acid (DSPA) multilamellar liposomes and stratum corneum lipid liposomes (SCLL). It was hoped that the studies with the latter would provide insights into the local nature of the actions of the n-alkanols as enhancers for the lipoidal pathway of the stratum corneum. For the purpose of estimating the changes in fluidity at different depths in these liposome bilayers, probes positioning at polar head group regions (1-anilinonaphthalene-8-sulfonic acid (ANS) and 5-(N-hexadecanoyl)aminofluorescein (HAF)), deep in the hydrophobic interior close to bilayer center (1,6-diphenyl-1,3,5-hexatriene (DPH)), and at graded depths (n-(9-anthroyloxy) fatty acids (n-AF)) were used. We tested the hypothesis that the appropriate microenvironment for transport is some region between the polar interface and the deep interior of the stratum corneum bilayers by examining the fluidity values obtained under the iso-enhancement conditions of $E = 10$ (i.e., 30% ethanol, 10% n-propanol, 2% n-butanol, and 1% n-pentanol).

Materials and Methods

Materials

Ethanol (US Industrial Chemical, Tuscula, IL), n-propanol, n-butanol, n-pentanol (Aldrich, Milwaukee, WI), borate buffer (pH 9.0) (Fisher, Pittsburgh, PA), and normal saline (McGaw, Irvine, CA) were used as received. The purity of the alkanol was checked using gas chromatography (methyl silicone gum HP-1 column in a Hewlett-Packard 5890 gas chromatograph) and was more than 98% pure in all cases. All other organic solvents were of analytical grade from various sources.

DPH, ANS, HAF, and n-AF (2 and 9-(9-anthroyloxy)stearic acids and 16-(9-anthroyloxy)palmitic acid) were purchased from Molecular Probes (Eugene, OR). Thin-layer chromatography of DPH and n-AF on silica gel plates developed in chloroform/methanol (90:10, v/v) showed only one spot for each probe as visualized by long UV light. Stock solutions of DPH and n-AF were prepared with N,N-dimethylformamide (EM Science, Cherry Hill, NJ) and methanol (Baker, Phillipsburg, NJ), respectively. ANS and HAF probes were used as received. Stock solutions of ANS and HAF were made in distilled water and dimethylsulfoxide (Mallinckrodt, Paris, KY), respectively. Stock solutions of all probes were kept in the dark until use.

Distearoylphosphatidylcholine (DSPC) and distearoylphosphatidic acid (DSPA) (Sigma, St. Louis, MO) were used as obtained from the supplier.

Preparation of liposomes and labeling of fluorescent probes

Stratum corneum lipid liposomes (SCLL) were prepared as described previously [19]. The liposomes contained 55% by weight epidermal ceramides, 25% cholesterol, 15% free fatty acids, and 5% cholesteryl sulfate (a close approximation to the composition of the human stratum corneum lipids). Six major ceramides and a mixture of free fatty acids form mostly saturated but heterogeneous microenvironments in the SCLL. SCLL were prepared by sonication at pH 9.0 (borate buffer). They were small unilamellar vesicles, ranging in size from 20 to 200 nm, and exhibited a final concentration of 3.6 mg lipid per ml. They remained stable for several weeks and showed a phase transition at 75°C which has been reported to be that of the mammalian stratum corneum intercellular lipid [20,56].

Phospholipid multilamellar liposomes were prepared by the method of Bangham et al. [21]. The lipids were dissolved in chloroform to give a 96:4 (DSPC/DSPA) molar ratio. The solutions were evaporated to dryness under a stream of nitrogen at 70°C (well above their phase transition temperature of 58°C) and the resulting thin lipid film was vacuum dried (10^{-4} Torr) for 1 to 2 h to remove the remaining chloroform. 5 ml of saline were added to give a final lipid concentration of 50 mM. The suspension was vortex-mixed and rapidly rotated (approx. 75 rpm) on a Buchi rotary evaporator at 70°C for 15 to 20 min. The MLV suspension was placed in a vial under nitrogen and cooled overnight. The MLV suspension vials were stored in a desiccator until use.

For fluorescence measurements, the SCLL or DSPC/DSPA liposomes were divided into two groups, one group with fluorescent probes and another without probes as light-scattering blanks. Fluorescent probes were added directly to each liposome solution containing an alkanol at a desired concentration. Liposomes with and without probes were incubated in a thermostatically controlled shaking water bath (Model YB-521, American Scientific, McGaw Park, IL) above their phase transition temperature (80°C for SCLL and 70°C for DSPC/DSPA liposomes) for at least 90 min in order to allow equilibration of probes with liposomes. It has been shown that the time required for complete uptake of probes into liposomes was less than 90 min [22,23].

In the experiments with DSPC/DSPA liposomes, the lipid-to-probe molar concentration ratios were 2000:1 for DPH, 100:1 for ANS, 1000:1 for HAF, and 300:1 for *n*-AF. In the experiments with SCLL, the lipid-to-probe concentration (w/v) ratios were 330:1 for DPH, 660:1 for HAF, and 25:1 for *n*-AF. Final concentrations of probes in the sample were less than 5 μM. It has been reported that at this final low concentration, the structural perturbation by *n*-AF in the bilayers might be insignificant [26,28]; also, experiment at 250:1 for *n*-AF with SCLL yielded essentially the same steady-state anisotropy results as at 25:1.

DPH is known to penetrate the hydrophobic interior and the orientation of this probe appears to depend critically on the physical state of the lipid bilayer [24,25]. Below the phase transition temperature of a lipid bilayer, DPH may orient perpendicularly to the plane of the bilayer while above the transition it may orient randomly [24]. Quantitative studies using the Förster resonance energy transfer methods have shown that, for egg lecithin bilayers (a heterogeneous internal environment), DPH was predominantly located at the center of the bilayer with the transverse orientation and, for dipalmitoylphosphatidylcholine (DPPC) bilayers, a fairly broad spread about the center was observed [25]. On the other hand, the location of ANS in a lipid bilayer is well established. For egg lecithin and DPPC bilayers, X-ray diffraction [26], NMR [27,28], and excitation energy transfer [29] studies have shown that ANS binds to the polar head groups and the positive charge of the choline residue appears to play an important role [30,31]. Also, an amphipathic probe like HAF which contains polar fluorescent head groups and nonpolar fatty acid tails locates at polar head group regions of dimyristoylphosphatidylcholine (DMPC) and plasma membrane vesicle bilayers [32]. A series of anthroyloxy fatty acid (*n*-AF) probes has been used for assessing fluidity changes at different depths in various bilayers. The relative positions have been established by fluorescence quenching [23,33], resonance energy transfer [33] and NMR [28] methods showing that *n*-AF do position their fluorophores at depths in bilayers depending on the point of attachment to the fatty acid chain.

Fluorescence measurements and data analysis

The fluorescence quantum yield of lipophilic probes such as DPH and *n*-AF is sensitive to the polarity of the probe's environment. In order to use this parameter as a measure of polarity, fluorescence emission spectra were recorded for each probe in hexadecane, liposomes, and aqueous buffer. All spectra were recorded at 37°C. Spectral integrals were determined by the method of Parker and Rees [36] to compute a quantum yield ratio for the probe in a lipophilic environment relative to buffer. In calculating this ratio, we used the spectral integral per mol of the probe instead of using the spectral integral per absorbance of the probe because of the significant differences and errors in absorbance among the samples. Lifetime measurements were made for DPH and *n*-AF in SCLL and hexadecane using an ISS K2 multifrequency phase and modulation fluorometer (ISS, Champaign, IL) equipped with frequency synthesizer (Marconi Instruments, Allendale, NJ) and an ISS-ADC interface for data collec-

tion and analysis. Samples were excited using the 325 nm line of an He-Cd Liconix model 4240NB laser (Liconix, Sunnyvale, CA). The phase shifts and demodulation factors were determined at 12 different modulation frequencies, logarithmically spaced (2, 3, 4.6, 7, 10.6, 16.2, 24.6, 37.4, 56.9, 86.5, 131.5 and 200 MHz). The fluorescence was measured at 37°C through a 375 nm cut-on filter in a filter channel. Fluorescence lifetimes were determined using a nonlinear least-squares program from ISS (ISS187) which minimized the reduced χ^2 (the squared deviations between the observed and calculated phase shifts and demodulation factors) for a goodness-of-fit. Following the detailed analysis procedure described before [34,35], a discrete multiexponential analysis and a continuous distribution analysis were compared on basis of the value of reduced χ^2.

Steady-state fluorescence spectra and anisotropy measurements were made with an ISS Greg 200 spectrofluorometer (ISS, Champaign, IL) in the photon counting mode.

For anisotropy determinations using ISSPC software (ISS, Champaign, IL), the fluorescence intensities were measured in the ratio mode through a polarizer oriented parallel ($I_{\parallel}$) or perpendicular ($I_{\perp}$) to the direction of polarization of the excitation light (the electrical vector of the excitation). The anisotropy (r) was calculated by

$$r = \frac{(I_{\parallel} - I^s_{\parallel}) - G(I_{\perp} - I^s_{\perp})}{(I_{\parallel} - I^s_{\parallel}) + 2G(I_{\perp} - I^s_{\perp})}$$

where I^s is the contribution of scattered light for an unlabeled liposome solution of the same composition as a reference and G is the grating correction factor representing the ratio of the sensitivities of the detection system for vertically and horizontally polarized light, which was measured using horizontally polarized excitation.

The light source for the steady-state fluorescence spectra and anisotropy measurements was a 300 W Xenon Arc lamp (ILC Technology, Sunnyvale, CA). Excitation wavelengths were 380 nm for ANS in DSPC/DSPA and 430 nm for ANS in SCLL, 490 nm for HAF, 360 nm for DPH, and 365 nm for *n*-AF. For anisotropy measurements, an L-format optical geometry was used, and fluoresence emission was collected through a cut-on filter, rather than a monochromator. The following cut-on filters were used; 455 for ANS, 400 for DPH, 515 for HAF, and 420 for *n*-AF. The temperature of the sample was maintained at 37°C using a circulating water bath (Techne, Princeton, NJ) and was checked by means of the Fisherbrand NIST thermometer with YSI probe (Fisher, Pittsburgh, PA).

Results and Discussion

Fluorescence emission maxima (λ_{max}) and quantum yield ratios (Qr)

Information on the polarity changes and the positions of the probes in the SCLL were obtained from the polarity sensitive parameters (i.e., λ_{max} and Q_r). The effects of solvent or microenvironment polarity on λ_{max} can be estimated from the Lippert equation which shows the relationship of the Stokes' shift to the orientation polarizability of the solvent molecule and the dipole moment change of the fluorophore during the excitation [51]. As the polarity of the microenvironment in a lipid bilayer increases, the Stokes' shift increases (i.e., red-shifted) towards lower energy. Q_r of a sample relative to the reference (each probe in buffer alone) was estimated from the Area Under the Curve (AUC) of the technical emission spectra. The absolute or relative quantum yield determinations using a refer-

TABLE I

Fluorescence emission maxima (λ_{max}) and quantum yield ratios (Q_r) data of n-AF and DPH in buffer, hexadecane and the stratum corneum lipid liposome (SCLL)

	Solution	2-AS		9-AS		16-AP		DPH	
		λ_{max} [a]	Q_r [b]	λ_{max}	Q_r	λ_{max}	Q_r	λ_{max}	Q_r
Without SCLL	buffer	475	1	461	1	470	1	– [c]	1
	hexadecane	448	15	441	20	450	23	430	101
With SCLL	buffer	456	11	440	14	450	11	429	88
	30% EtOH	456	9	440	10	450	9	429	43
	10% n-POH	456	11	440	17	450	19	429	118
	2% n-BtOH	456	11	440	17	450	15	429	107
	1% n-PtOH	456	12	440	19	450	11	429	119

[a] nm.

[b] Calculated from the Area Under the Curve (AUC) of emission spectra: $Q_r = (AUC_x/mol)/(AUC_o/mol)$ where the subscripts, x and o, represent any sample and buffer solution (without SCLL) of each probe.

[c] Very weak fluorescence.

ence fluorophore with a known absolute quantum yield was not made. Therefore, the measured Q_r values were used only for purposes of internal comparisons. Also, the Raman spectrum was measured with buffer alone and the contribution of this to the fluorescence spectra for each probe in buffer was less than 3%.

As shown in Table I, when *n*-AF and DPH were in the nonpolar solvent, hexadecane, or incorporated into the SCLL, Q_r values were significantly increased and the technical emission spectra were blue-shifted relative to those in buffer. This is probably attributable to the increased hydrophobicity of the microenvironments of the fluorophores. Although there were some variations in the Q_r values with the n-alkanols in the SCLL, it may be concluded from the Q_r and λ_{max} results that the n-alkanols under iso-enhancement conditions do not appear to significantly alter the polarity of the microenvironment in the SCLL, which (as will be seen) is consistent with the lifetime results. Furthermore, when λ_{max} values in the SCLL were compared with those in hexadecane, all the probes showed the same λ_{max} values (except 2-AS which was red-shifted by 8 nm) in the SCLL. For the 2-AS case, the result suggested that the probe was located near the polar interface and was accessible to water.

Fluorescence lifetimes

Fluorescence lifetime data are presented in Table II for DPH and *n*-AF in hexadecane and the SCLL. Lifetime measurements were determined at 37°C where the SCLL are in the gel state.

On the basis of the statistical criteria (reduced χ^2) showing a goodness-of-fit, the measured phase shifts and demodulation factors were analyzed in terms of discrete multiexponentials and continuous distribution functions. For all the probes used in this study, the discrete monoexponential and the unimodal distribution fits showed much higher reduced χ^2 values (> 50) than the double exponential fits (reduced $\chi^2 = 1$ to 2). Furthermore, bimodal distributions and more complex functions were not statistically better than the discrete biexponential function. We judged from these analyses that the discrete biexponential function with the minimum of free parameters was a good model.

Most of the membrane-bound fluorescent probes including DPH and *n*-AF are known to display complex fluorescence decay characteristics. The subject of multiexponential decay of DPH fluorescence and the existence of a short lifetime component (less than 2 or 3 ns) has been controversial. In the case of DPH, the origin of a second, short lifetime has been attributed to irreversible photolytic damage [44,45] or reversible photobleaching [46,47] of DPH fluorescence due to the prolonged exposure of the lipid or DPH to exciting light. Recently, however, Lentz [12] suggested that all of the anomalous spectral properties and fluorescence decay of DPH (or of a DPH-derivatives) were consistent with a dual-excited states (^{1}Ag*, ^{1}Bu*) model. In

TABLE II

Fluorescence lifetime data for n-AF and DPH in the stratum corneum lipid liposomes (SCLL) and hexadecane

Probe		Alkanol	τ_1 [a] (ns)	f_1 [b]	τ_2 (ns)	f_2	$\langle\tau\rangle$ [c] (ns)	red. χ^2 [d]
2-AS	SCLL	none [e]	4.92	0.72	0.71	0.28	3.74	0.7
		30% EtOH	5.15	0.72	0.50	0.28	3.85	1.5
		10% n-POH	5.08	0.75	0.67	0.25	3.98	1.6
		2% n-BtOH	5.03	0.72	0.71	0.28	3.82	1.3
		1% n-PtOH	5.00	0.73	0.70	0.27	3.84	1.7
	Hexadecane		12.43	0.73	1.19	0.27	9.40	2.0
9-AS	SCLL	none [e]	8.29	0.72	1.21	0.28	6.31	1.2
		30% EtOH	7.82	0.73	0.55	0.27	5.86	0.9
		10% n-POH	8.30	0.74	0.81	0.26	6.35	1.3
		2% n-BtOH	8.50	0.76	0.90	0.24	6.68	1.5
		1% n-PtOH	8.80	0.75	0.78	0.25	6.79	1.9
	Hexadecane		9.21	0.78	1.15	0.22	7.44	1.0
16-AP	SCLL	none [e]	11.88	0.87	0.73	0.13	10.43	1.0
		30% EtOH	10.87	0.86	0.54	0.14	9.42	1.7
		10% n-POH	11.51	0.82	0.71	0.18	9.57	1.5
		2% n-BtOH	11.90	0.88	0.82	0.12	10.57	1.2
		1% PtOH	11.30	0.89	0.70	0.11	10.13	1.8
	Hexadecane		11.00	0.88	0.80	0.12	9.78	1.0

[a] Fluorescence lifetime.
[b] Fraction of each lifetime component.
[c] Average lifetime, $\langle\tau\rangle = f_1\tau_1 + f_2\tau_2$.
[d] Reduced χ^2, the squared deviations between the observed and calculated phase shift and demodulation factor.
[e] Buffer alone.

DPH, the $^1Ag^*$ state is slightly lower in energy than the $^1Bu^*$ state (ΔE = 0.4 to 2.4 kcal/mol), and excitation is via the symmetry-allowed ^1Ag-$^1Bu^*$ transition, while emission is a mixture of a relatively strong, symmetry-forbidden (long lifetime) $^1Ag^*$-^1Ag fluorescence and weaker, symmetry-allowed (short lifetime) $^1Bu^*$-^1Ag fluorescence [48]. Therefore, DPH in membranes exhibits a long lifetime (8 to 12 ns) from the $^1Ag^*$-^1Ag transition and a shorter lifetime (close to 1 ns) from the $^1Bu^*$-^1Ag transition [49]. Also, it has been reported [49] that, as the concentration of DPH increases (higher than 10^{-5} M), DPH dimerizes to allow more rapid decay of $^1Ag^*$-^1Ag fluorescence (2 to 3 ns). In the present study, the final concentration of DPH was much lower than 10^{-5} M and thus the origin of a short lifetime of DPH in the SCLL may not be due to the dimerization of DPH. From these considerations, the biexponential decay behavior of DPH in the SCLL or even in hexadecane as shown in Table II appears reasonable and the short lifetime components (close to 1 ns) may result from the $^1Bu^*$-^1Ag fluorescence.

Heterogeneity analyses of *n*-AF by Matayoshi and Kleinfeld [50] demonstrated that the decay of *n*-AF in the phospholipid liposomes or in nonpolar solvents was also biexponential. These investigators proposed two discrete excited states (S_1^{FC}, S_1^{EQ}) which are different in molecular configuration. The S_1^{FC} (first excited state, Franck-Condon geometry)-S_1^{EQ} (first excited state, equilibrium geometry) transition involves an intramolecular relaxation process occurring during the lifetime scale. They associated a short lifetime component (1 to 2 ns) with S_1^{FC} and a longer component with S_1^{EQ}. Their results also showed that photobleaching or the presence of a microheterogeneous site was not a probable origin of the short lifetime component for *n*-AF.

Two lifetime components were observed in all of our lifetime measurements (Table II). In the case of *n*-AF, the longer lifetime accounted for 70–80% of the observed fluorescence, and 80–90% in the case of DPH. The n-alkanols had no significant effects on the mean lifetimes or on the fractions of the lifetimes of all the probes. However, a gradual increase in lifetime was observed as the probe moved deeper towards the bilayer center (3–4 ns at C2, 6–7 ns at C9, 7–9 ns at C16, and 9–11 ns at the bilayer center). Also, the lifetime of 2-AS was significantly lower in the SCLL than in hexadecane. This is probably due to the close proximity of 2-AS to the polar headgroups. The lifetimes of *n*-AF and DPH are known to be strongly dependent upon the dielectric constant (polarity) of the solvents but independent of the viscosity [12].

Therefore, in summary, it may be stated that firstly, there exists a polarity gradient in the SCLL bilayer, the polarity decreasing with depth in the bilayer; secondly, the n-alkanols under iso-enhancement conditions do not appear to change the polarity in the SCLL; thirdly,

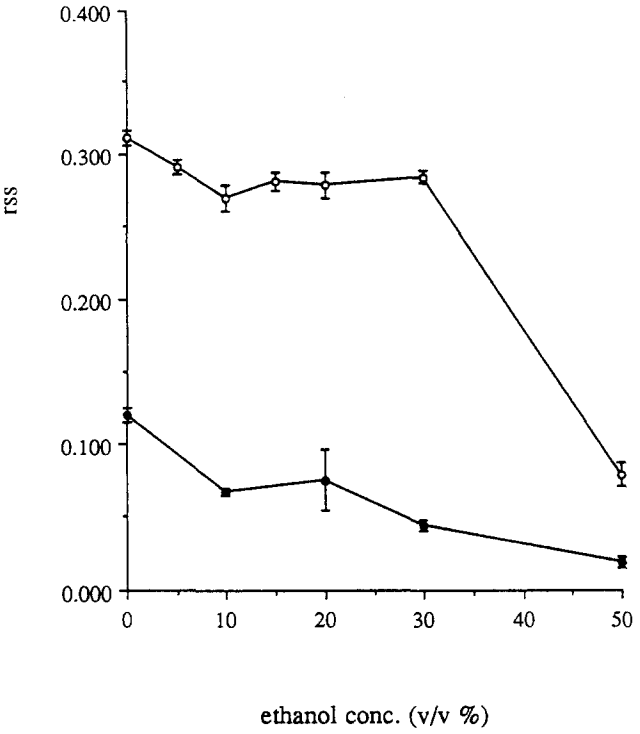

Fig. 1. Steady-state anisotropy (r_{ss}) of DPH (open symbols) and ANS (closed symbols) as a function of the ethanol concentration in the DSPC/DSPA liposomes.

these results are consistent with the fluorescent probes positioning at graded depths in the bilayer; fourthly, the n-alkanols do not significantly alter the fluorescent lifetimes of the probes positioned in the SCLL and therefore the steady-state anisotropy, r_{ss}, values may be directly associated with fluidities of the microenvironments. From this, it may be concluded that fluorescent probe studies with *n*-AF and DPH positioned at a graded depths, from the lipid/water interface to the bilayer center, may yield information on the fluidity and polarity of the microenvironment where they are located in the SCLL.

Steady-state anisotropy

DSPC / DSPA multilamellar liposomes. Changes in the steady-state anisotropy (r_{ss}) with changes in the alkanol concentration using DPH as a hydrophobic probe and ANS as a polar head group region probe with DSPC/DSPA multilamellar liposomes as a model bilayer consisting of saturated and homogeneous alkyl chains are shown in Figs. 1–4. The r_{ss} was measured at 37°C which is below the phase transition temperature (55°C).

With ethanol (Fig. 1), r_{ss} for DPH decreased monotonically up to 10%, leveled off at the higher concentrations (15–30%), and then dropped off sharply at 50% ethanol. Quasi-elastic light scattering and vesicular permeability studies (unpublished data) showed that 50% ethanol dissolves or lyses these liposomes. The r_{ss}

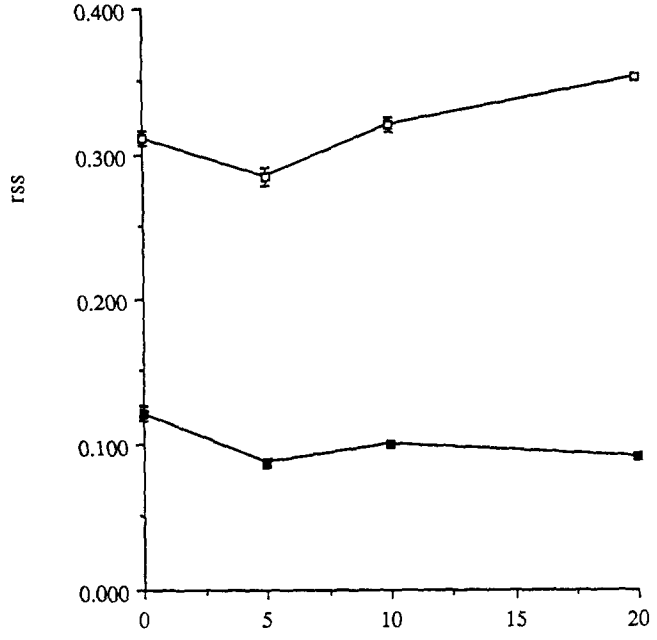

Fig. 2. Steady-state anisotropy (r_{ss}) of DPH (open symbols) and ANS (closed symbols) as a function of the n-propanol concentration in the DSPC/DSPA liposomes.

values for ANS decreased monotonically up to 50%.

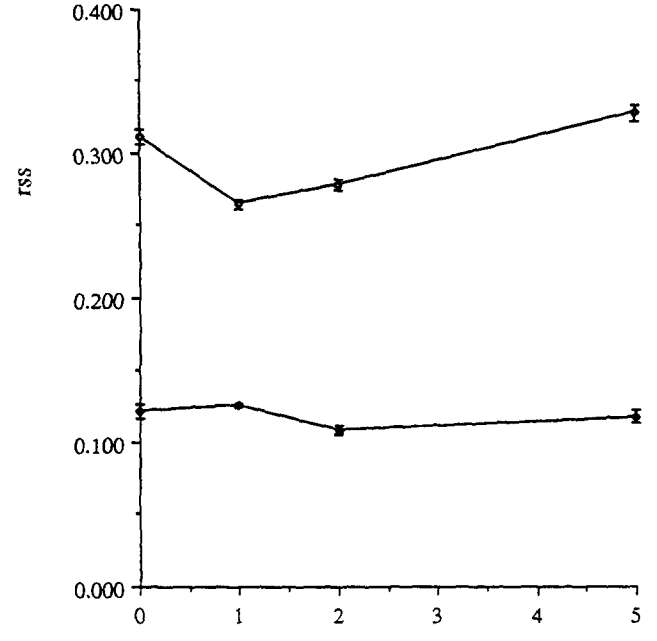

Fig. 3. Steady-state anisotropy (r_{ss}) of DPH (open symbols) and ANS (closed symbols) as a function of the n-butanol concentration in the DSPC/DSPA liposomes.

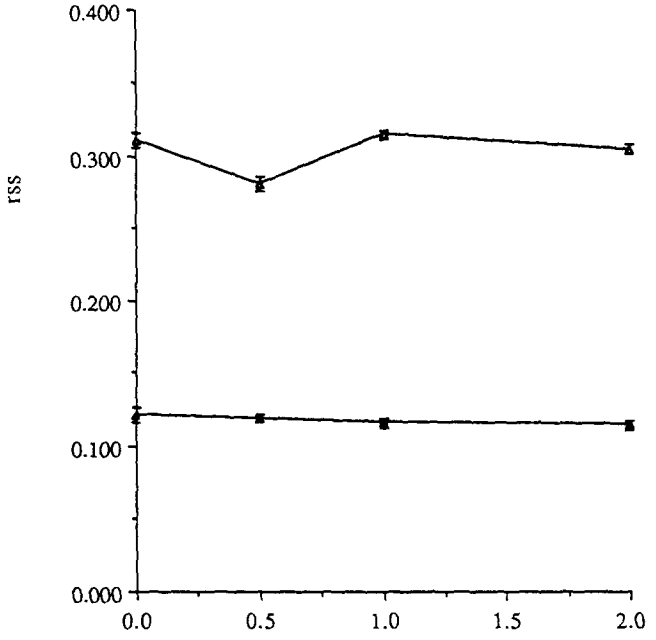

Fig. 4. Steady-state anisotropy (r_{ss}) of DPH (open symbols) and ANS (closed symbols) as a function of the n-pentanol concentration in the DSPC/DSPA liposomes.

The results obtained with n-propanol, n-butanol, and n-pentanol (Figs. 2–4) were similar. The r_{ss} for DPH exhibited a modest biphasic pattern in each instance and the r_{ss} values for ANS were relatively constant over the concentration ranges investigated.

The percent change in r_{ss} for DPH and ANS for each of the n-alkanols at iso-enhancement concentrations (i.e., 30% ethanol, 10% n-propanol, 2% n-butanol. and 1% n-pentanol) is presented in Table III. Positive values represent decreases in anisotropy in the presence of the n-alkanols, indicating increases in fluidity. The increases in fluidity at the polar interface (ANS results) decreased with increasing chain length of the n-alkanols: the largest increase in fluidity here took place with 30% ethanol, the effects were only about

TABLE III

Percent change in the steady-state anisotropy (r_{ss} (%)) of DPH and ANS induced by the n-alkanols under iso-enhancement (E = 10) conditions in the DSPC/DSPA liposomes

r_{ss} (%) = [(r_{ss} (buffer) − r_{ss} (alkanol))/r_{ss} (buffer)] × 100.

Alkanol	r_{ss} (%)	
	ANS	DPH
30% ethanol	63.3	8.7
10% n-propanol	16.7	−2.9
2% n-butanol	10.0	10.9
1% n-pentanol	3.3	−1.3

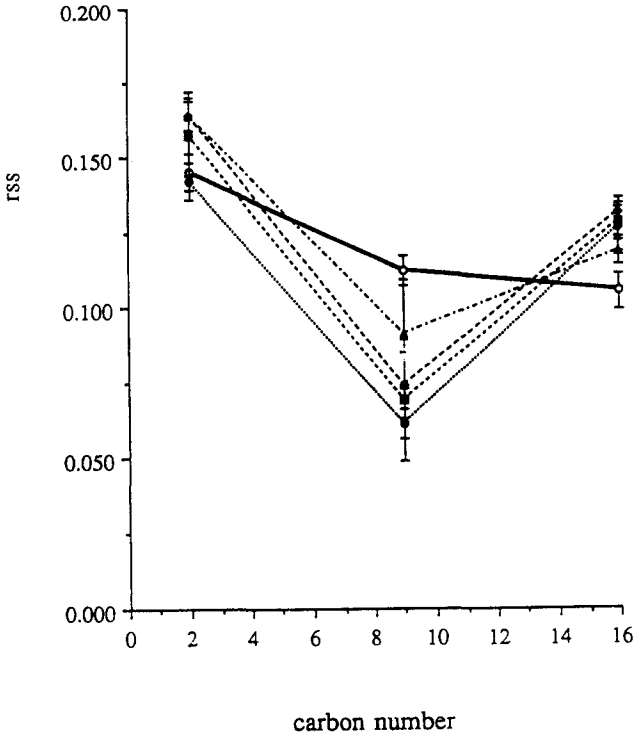

Fig. 5. Depth-dependent effects of the n-alkanols under iso-enhancement ($E = 10$) conditions on the steady-state anisotropy (r_{ss}) obtained with *n*-AF (2-AS, 9-AS and 16-AP) in the DSPC/DSPA liposomes. Symbols: open circles (buffer); closed circles (30% ethanol); closed squares (10% n-propanol); closed diamonds (2% n-butanol); closed triangles (1% n-pentanol). The means of the r_{ss} values in the presence of n-alkanols (closed symbols) were statistically different from those in buffer (open symbol), $P < 0.05$, Student's *t*-test, except in 30% ethanol at C-2 region.

one-fourth as large with 10% n-propanol and they diminished even further with n-butanol and n-pentanol. Fluidity changes in the deeper hydrocarbon region close to the bilayer center were not indicated by the DPH results under iso-enhancement ($E = 10$) conditions.

Assessment of the depth-dependent effects of the n-alkanols was made using *n*-AF (2-AS, 9-AS, and 16-AP). As shown in Fig. 5, there was a modest fluidity gradient for the DSPC/DSPA liposomes going from the polar interface towards the bilayer center, which is consistent with ESR [37] and ^{2}H-NMR [38] results obtained with DPPC liposomes. All the n-alkanols under iso-enhancement conditions exhibited similar effects, with the largest increase in fluidity occurring in the middle region (C9). Near the polar interface (C2) and near the lipid bilayer center (C16), the fluidities appeared to decrease somewhat when the n-alkanols at iso-enhancement concentrations were added.

The biphasic anisotropy profiles for DPH as a function of the alkanol concentration (Figs. 1–4) and the decreased fluidity at C2 and near the bilayer center (C16) (Fig. 5) would be consistent with the induction of an interdigitated gel phase ($L_\beta I$) in the presence of the short chain n-alkanols. Interdigitation has been a well recognized phenomenon for saturated symmetric and asymmetric phospholipid bilayers [39–41]. These alkanols may intercalate and perturb the regions between polar head groups and/or slightly below polar head groups. The consequential increase in the interfacial area makes voids within the bilayer core and thus two apposing hydrocarbon chains may interdigitate to minimize free energy [41]. This interdigitation behavior depends on the concentrations of the alkanols [42,43]. At relatively high concentrations (higher than 10% ethanol, 5% n-propanol, 1% n-butanol, and 0.5% n-pentanol), there might be abrupt decreases in the bilayer thickness and increases in the order (packing density) of the lipid alkyl chains in the DSPC/DSPA liposomes.

Stratum corneum lipid liposomes (SCLL). HAF rather than ANS was used as a polar interface region probe since it was found that ANS did not bind well to the SCLL as indicated by very low fluorescence intensity. As mentioned before, the positive charge of the choline moiety may be required for the binding of ANS to the lipid bilayers. Therefore, ANS binds well to phosphatidylcholine and sphingomyelin which contain choline moieties but does not bind well to the other lipids such as phosphatidylserine, phosphatidylinositol, phosphatidic acid, cardiolipin, and gangliosides [30,31]. Thus, the poor binding of ANS to the SCLL is probably due to the lipid composition of the SCLL (i.e., ceramides, free fatty acids, cholesterol, and cholesteryl sulfate).

In the present study, the r_{ss} was measured with HAF in the SCLL and DSPC/DSPA liposomes and compared with ANS in the DSPC/DSPA liposomes. The effects of 30% ethanol in increasing the fluidity of the polar interface region were similar for the SCLL (70% change in r_{ss} with HAF) and the DSPC/DSPA liposomes (59% with HAF). Also, HAF appeared to sense the same microenvironment as ANS with the DSPC/DSPA liposomes (63%).

The fluidity changes in the polar interface region (HAF results) and the deep hydrocarbon interiors (DPH results) caused by the n-alkanols with the SCLL under iso-enhancement conditions are shown in Table IV. These results obtained with the SCLL were very similar to those obtained with the DSPC/DSPA liposomes (see Table III). The data are consistent with the view that, under iso-enhancement conditions, the increases in fluidity at the polar interface decrease as the carbon number of the n-alkanol increases. Although the effects were small, there appeared to be some increase in fluidity in the deep hydrocarbon region of the SCLL with all the n-alkanols at iso-enhancement concentrations.

The steady-state anisotropy data obtained for *n*-AF in the SCLL are presented in Fig. 6. The r_{ss} patterns

TABLE IV

Percent change in the steady-state anisotropy (r_{ss} (%)) of DPH and HAF induced by the n-alkanols under iso-enhancement (E = 10) conditions in the SCLL

r_{ss} (%) = [(r_{ss} (buffer) − r_{ss} (alkanol))/r_{ss} (buffer)] × 100.

Alkanol	r_{ss} (%)	
	HAF	DPH
30% ethanol	70.8	9.3
10% n-propanol	28.5	10.5
2% n-butanol	6.9	5.2
1% n-pentanol	5.6	12.0

with the SCLL differ significantly from those of the DSPC/DSPA liposomes (see Fig. 5). First, in buffer only, there was little or no change in fluidity in the C2–C9 region, followed by a large increase in fluidity at C16 for the SCLL, while there was a more modest and gradual increase in fluidity for the DSPC/DSPA liposomes over this range. This result may be due to the heterogeneous (varying chain length) lipid composition of the SCLL. Most of the significant changes in fluidity caused by the n-alkanols occurred at the intermediate depths (C2–C9) and there were no significant changes in fluidity in the bilayer center region (C16). In the upper region (C2), the largest fluidity increase was obtained with 30% ethanol and as the chain length of the n-alkanol increased, the increases in the fluidity decreased. The opposite result was obtained in the middle region (C9) with 1% n-pentanol showing the largest fluidity increase.

Quantification of the fluidity parameters from the steady-state anisotropy (r_{ss}) and lifetime (τ) data in the SCLL

As mentioned in the Introduction, r_{ss} may be resolved into the two components, a static part (r_∞), which is proportional to the square of the order parameter, and a dynamic part (r_f), which is related to the

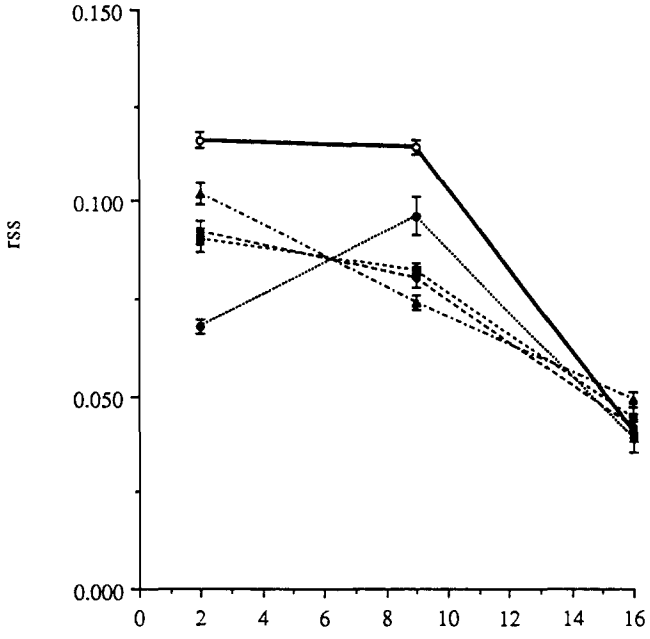

Fig. 6. Depth-dependent effects of the n-alkanols under iso-enhancement ($E = 10$) conditions on the steady-state anisotropy (r_{ss}) obtained with *n*-AF (2-AS, 9-AS and 16-AP) in the SCLL. Symbols: open circles (buffer); closed circles (30% ethanol); closed squares (10% n-propanol); closed diamonds (2% n-butanol); closed triangles (1% n-pentanol).

rotational correlation time and proportional to the microviscosity [10,16,17]. For the purpose of quantification, it is assumed that the r_{ss} of DPH is mainly determined by its static component (r_∞) while that of *n*-AF is assumed to predominantly reflect the dynamic component (r_f). Therefore, it is believed reasonable to assume that the fluidity parameters for DPH are inversely proportional to the 'order parameter (S)' (i.e., lipid packing density) and those for *n*-AF are inversely proportional to the 'rotational correlation time (ϕ)' (and proportional to the microviscosity); time-resolved

TABLE V

Effects of the n-alkanols at the iso-E concentrations on the fluidity parameters obtained with DPH in the straum corneum lipid liposomes (SCLL)

Alkanol	r_{ss} [a]	r_∞ [b]	S [b]	r_∞ [c]	S [c]
None [d]	0.248 ± 0.005	0.231	0.777	0.223	0.763
30% EtOH	0.225 ± 0.008	0.200	0.722	0.192	0.708
10% n-POH	0.222 ± 0.007	0.196	0.716	0.188	0.701
2% n-BtOH	0.235 ± 0.003	0.213	0.746	0.206	0.733
1% n-PtOH	0.178 ± 0.010	0.137	0.598	0.131	0.585

[a] Steady-state anisotropy. Means and standard deviations of five determinations with three independent experiments.

[b] Limiting hindered anisotropy (r_∞) and order parameter (S) calculated from the empirical relationship of r_∞ to r_{ss} (Van Blitterswijk et al. [16]): $r_\infty = (4/3)r_{ss} - 0.10$ for $0.13 < r_{ss} < 0.28$ and $S^2 = r_\infty / r_o$ where r_o is the maximum anisotropy (0.383).

[c] Calculated from the empirical relationship of r_∞ to r_{ss} (Van der Meer et al. [17]): $r_\infty = r_o r_{ss}^2 / [r_o r_{ss} + (r_o - r_{ss})^2 / m]$ where $r_o = 0.386$ and $m = 1.71$ for DPH.

[d] Buffer alone.

anisotropy decay studies should be helpful in more firmly establishing this approach.

As shown in Table V, the r_∞ values of DPH in the SCLL were estimated from the two empirical relationships of r_{ss} to r_∞, which were theoretically derived and experimentally verified [16,17]. Furthermore, estimated r_∞ values were used to calculate the order parameter, S (square root of r_∞/r_o, where r_o is the maximum anisotropy of DPH). It could be seen in Table V that, firstly, r_∞ values were close to r_{ss} values, which suggests that the static component contributed significantly to the observed anisotropy; secondly, the two empirical relationships gave very similar values for the order parameter; thirdly, the n-alkanols appeared to have induced decreases in the order parameter (i.e., decreased lipid packing density), especially with n-pentanol.

The order parameter, S, referred to here may be associated with that defined and used in ^{2}H-NMR and ESR techniques. However, it should be mentioned that in the case of DPH, it represents the local order of the average location of DPH in the SCLL, while in the case of ^{2}H-NMR and ESR studies, it is the local order parameter of a particular alkyl chain segment [16]. It has been shown that S values of DPH agree with ^{2}H-NMR values of C10–C12 regions with the DPPC liposomes [10].

Table VI shows the results with *n*-AF in the SCLL. The rotational correlation times (ϕ) and the consequent rotational rates (R) in Table VI represent the mean values (actually, harmonic mean for ϕ and arithmatic mean for R) since most of the membrane-bound probes have two ϕ values which cannot be resolved from the steady-state measurement and the Perrin equation. In the present study, $<\phi>$ and $<R>$ were calculated from the Perrin equation under the assumption of no hindered rotation ($r_\infty = 0$). The reasons for this assumption are as follows: *n*-AF is expected to have two rotational modes (i.e., in-plane rotation (hindered) and out-of-plane rotation (unhindered)) and these two modes are dependent on the excitation wavelength [7]. However, there is evidence that the rotation of *n*-AF at the excitation wavelength (365 nm) used in this study is unhindered ($r_\infty = 0$) [52]. As mentioned before, two empirical relationships for *n*-AF have been developed, which relate r_{ss} to r_∞ [17,18]. However, it should be mentioned that both empirical relationships were obtained from r_{ss} and r_∞ data measured at longer excitation wavelengths (around 380 nm). At this excitation wavelength, hindered in-plane rotations are mainly detected [7]. Therefore, the r_∞ values calculated from the r_{ss} values (measured at 365 nm) using these empirical equations may be overestimated. The time-resolved anisotropy decay or the differential phase measurements may be employed for determining the values for ϕs and r_∞. However, for a probe with two correlation times and hindered rotation, it may not be easy matter to obtain the accurate and reliable values from the time-resolved measurements.

As can be seen in Table VI and plotted in Fig. 7,

TABLE VI

Effects of the n-alkanols on the fluidity parameters obtained with n-AF in the stratum corneum lipid liposomes (SCLL)

Probe	Alkanol	r_{ss} [a]	$\langle\tau\rangle$ [b] (ns)	$\langle\phi\rangle$ [c] (ns)	$\langle R\rangle$ [d] (ns^{-1})
2-AS	none [e]	0.116±0.002	3.74	3.81	0.044
	30% EtOH	0.068±0.002	3.85	1.62	0.103
	10% n-POH	0.090±0.003	3.98	2.56	0.065
	2% n-BtOH	0.092±0.003	3.82	2.55	0.065
	1% n-PtOH	0.102±0.003	3.84	3.06	0.054
9-AS	none [e]	0.114±0.002	6.31	6.20	0.027
	30% EtOH	0.096±0.005	5.86	4.20	0.040
	10% n-POH	0.082±0.002	6.35	3.52	0.047
	2% n-BtOH	0.080±0.002	6.68	3.56	0.047
	1% n-PtOH	0.074±0.0002	6.79	3.22	0.052
16-AP	none [e]	0.041±0.003	7.73	1.68	0.099
	30% EtOH	0.039±0.004	8.11	1.66	0.100
	10% n-POH	0.044±0.003	7.91	1.87	0.089
	2% n-BtOH	0.042±0.002	8.25	1.84	0.091
	1% n-PtOH	0.049±0.002	8.42	2.27	0.073

[a] Steady-state anisotropy. Means and standard deviations of five determinations with three independent experiments.

[b] Average fluorescence lifetime. Two lifetime components were measured for all the probes (biexponential decay). $\langle\tau\rangle = f_1\tau_1 + f_2\tau_2$ where f and τ represent the fractional intensity and lifetime of each component.

[c] Average rotational correlation time calculated from the Perrin's equation under the assumption of no steric hindrance in the probe rotation: $\langle\phi\rangle = \langle\tau\rangle/((r_o/r_{ss})-1)$ where r_o is the maximum anisotropy (0.23 [7]).

[d] Average rotational rate (average of in-plane and out-of-plane rotations of probe). $\langle R\rangle = 1/(6\langle\phi\rangle)$.

[e] Buffer alone.

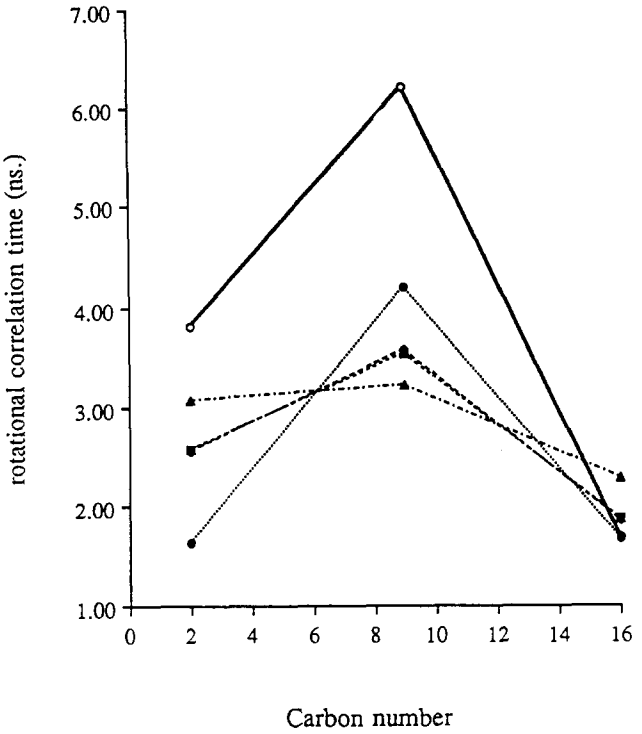

Fig. 7. Effects of the n-alkanols under iso-enhancement (E = 10) conditions on the average rotational correlation time ($< \phi >$) obtained with *n*-AF (2AS, 9AS, and 16AP) in the SCLL. Symbols: open circles (buffer); closed circles (30% ethanol); closed squares (10% n-propanol); closed diamonds (2% n-butanol); closed triangles (1% n-pentanol).

$< \phi >$ in buffer increased from C2 (3.81 ns) to C9 (6.20 ns) and then decreased dramatically at C16 region (1.68 ns). This result suggests that in the SCLL the most viscous (ordered) region is at the middle depths and the most fluid region near the bilayer center. The decreases in r_{ss} caused by the n-alkanols at C2 and C9 regions may be interpreted to be mainly due to the decreased rotational correlation time (or increased rotation rate of the fluorophore) since there were no significant changes in lifetimes. Calculated values of $< R >$ as a fluidity parameter for *n*-AF in the SCLL showed around 2-fold increases in fluidity by the n-alkanols under iso-enhancement conditions at the intermediate depths (C2–C9) and no changes in fluidity near the bilayer center; 30% ethanol showed the biggest effect at the C2 region and 1% n-pentanol at the C9 region.

Relationship of this work to the mechanism(s) of stratum corneum transport enhancement induced by the n-alkanols

First, lipid extraction has been suggested as the principal mechanism by which n-alkanols enhance percutaneous absorption for the lipoidal pathway of the stratum corneum [53]. However, at least in hairless mouse skin studies, we have shown that (a) exposure of hairless mouse skin to aqueous alkanols at iso-enhancement ($E = 10$) concentrations do not cause irreversible changes and (b) size changes (measured by quasi-elastic light scattering) of SCLL induced by the n-alkanols are reversed upon dilution. Therefore, lipid extraction cannot explain the effects of the alkanols as transport enhancers at these modest n-alkanol levels and the likely explanation resides in some kind of reversible interaction between the n-alkanols and the stratum corneum lipid bilayers.

The present work and earlier FTIR studies suggest the interaction between the n-alkanols and the stratum corneum lipids does not lead to gross lipid alkyl fluidization but rather to a 'local' increase in fluidity near the polar interface and/or in a region of intermediate depth from the polar interface. The FTIR studies of the effects of the short chain n-alkanols at iso-enhancement concentrations on the stratum corneum lipid and phospholipid alkyl chain packing, mobility, and conformational order have provided no evidence for gross lipid alkyl chain fluidization in the gel phase by the n-alkanols. These investigations suggested therefore that possible mechanism(s) may involve (a) the polar head region, (b) the interfacial regions between possible interdigitated and noninterdigitated phases resulting from the gel phase segregation, and (c) low populations of highly mobile gel or liquid-crystalline phases [5,6].

The present fluorescence anisotropy study supports this view that the appropriate microenvironment (primary action site) in the stratum corneum lipid bilayer for transport enhancement of lipophilic drugs induced by short chain n-alkanols is the intermediate depth region (C2–C9), where the lipid alkyl chains are highly ordered and densely packed, rather than the deep hydrophobic interior. The n-alkanols, at iso-enhancement ($E = 10$) concentrations, induced increases in fluidity of around a factor of two in this intermediate depth region and caused small increases in fluidity in the region near the bilayer center. Thus, the E values are not quantitatively proportional to the fluidity values. Possible reasons for this are the following: (a) it is not clear whether the rotational motion of the fluorophore should be a correlate of the translational diffusion of a permeant. The 'cavity volume' involved in the rotational motion of the fluorophore might be significantly smaller than the 'free volume' required for diffusion of large steroid molecules; (b) the enhancement factor, E, may be dependent on the molecular size of the permeant; Liu [55] found that large steroids like β-estradiol, estrone, and hydrocortisone were enhanced 10-fold by 30% ethanol whereas ethanol as a permeant was enhanced only 2- to 3-fold; (c) the enhancement factor accounts for both the permeant's partitioning tendency and diffusivity [1]; it is expected that lipid fluidization by the n-alkanols in the rate-

limiting microenvironment would increase both the partitioning tendency and diffusivity for a permeant, yielding a squaring effect upon E.

The present data do not support the view that interdigitation is of great importance in the interaction of the n-alkanols with SCLL. Firstly, DPH results in Table IV showed no increased order under iso-enhancement conditions and the profile of r_{ss} as a function of the ethanol concentration showed no biphasic effect (data not given); secondly, there was no decreased fluidity in the presence of the n-alkanols near the bilayer center, which is expected for the interdigitation phenomena; thirdly, the ethanol induction of the interdigitated gel phase is known to be prevented by the presence of 20 mol% or higher cholesterol [39]. The SCLL contains approx. 25% cholesterol.

A probable mode of action of short chain alkanols in the enhancement of the lipoidal pathway for permeation may therefore involve the polar head region of the bilayer or the region slightly below this polar head plane (intermediate depths, C2–C9) or both. Anderson and Raykar [54] have pointed out that permeant functional group contributions to permeant transport across stratum corneum are most consistent with the rate-limiting microenvironment being significantly more polar than would be the case for pure hydrocarbon. Short chain n-alkanols may solvate the lipid/water interface, intercalating and disrupting the interactions of the upper regions of alkyl chains and the interactions between the polar head groups. This could result in an increase in the effective interfacial area, increases in fluidity of the lipid alkyl chain, and thereby an increase in both diffusivity and partitioning tendency for a permeant in these microenvironments of the stratum corneum lipid bilayers.

Acknowledgments

This research was supported in part by Ciba-Geigy, Inc. and NIH grant GM43181. The authors would like to thank Dr. Vladimir Hlady for his help with fluorescence lifetime measurements and the Center for Biopolymers at Interfaces for the use of the spectrofluorometers.

References

1 Kim, Y.H., Ghanem, A.H., Mahmoud, H. and Higuchi, W.I. (1992) Int. J. Pharm. 80, 17–31.
2 Ghanem, A.H., Mahmoud, H., Higuchi, W.I., Liu, P. and Good, W.R. (1992) Int. J. Pharm. 78, 137–156.
3 Kim, Y.H., Ghanem, A.H., Mahmoud, H., Higuchi, W.I., Kurihara-Bergstrom, T. and Good, W.R. (1989) Pharm. Res. 6 (Suppl.), S100.
4 Ghanem, A.H., Mahmoud, H., Higuchi, W.I., Rohr, U.D., Borsadia, S., Liu, P., Fox, J.L. and Good, W.R. (1987) J. Controlled Release 6, 75–83.
5 Knutson, K., Krill, S.L. and Zhang, J. (1990) J. Controlled Release 11, 93–103.
6 Krill, S.L. (1989) Ph.D. Dissertation, The University of Utah, Utah.
7 Vincent, M. and Gallay, J. (1984) Biochemistry 23, 6514–6522.
8 Collins, J.M. and Grogan, W.M. (1991) Biochim. Biophys. Acta 1067, 171–176.
9 Prendergast, F.G., Haugland, R.P. and Callahan, P.J. (1981) Biochemistry 20, 7339–7345.
10 Jahnig, F. (1979) Proc. Natl. Acad. Sci. USA 76, 6361–6365.
11 Kinosita, K., Kawato, S. and Ikegami, A. (1977) Biophys. J. 20, 289–305.
12 Lentz, B.R. (1988) in Spectroscopic Membrane Probes (Loew, L.M., ed.), Vol. I, pp. 13–41, CRC press, Boca Raton.
13 Dale, R.E., Chen, L.A. and Brand, L. (1977) J. Biol. Chem. 252, 7500–7510.
14 Thulborn, K.R. and Beddard, G.S. (1982) Biochim. Biophys. Acta 693, 246–252.
15 Hare, F., Amiel, J. and Lussan, C. (1979) Biochim. Biophys. Acta 555, 388–408.
16 Van Blitterswijk, W.J., Van Hoeven, R.P. and Van der Meer, B.W. (1981) Biochim. Biophys. Acta 644, 323–332.
17 Van der Meer, B.W., Van Hoeven, R.P. and Van Blitterswijk, W.J. (1986) Biochim. Biophys. Acta 854, 38–44.
18 Kutchai, H., Chandler, L.H. and Zavoico, G.B. (1983) Biochim. Biophys. Acta 736, 137–149.
19 Abraham, W. and Downing, D.T. (1989) J. Invest. Dermatol. 93, 809–813.
20 Wertz, P.W., Abraham, W., Landmann, L. and Downing, D.T. (1986) J. Invest. Dermatol. 87, 582–584.
21 Bangham, A.D., Hill, M.W. and Miller, N.G.A. (1974) in Methods in Membrane Biology (Korn, E.D., ed.), Vol. 1, pp. 1–68, Plenum Press, New York.
22 Lentz, B.R., Barenholz, Y. and Thompson, T.E. (1976) Biochemistry 15, 4521–4528.
23 Thulborn, K.R. and Sawyer, W.H. (1978) Biochim. Biophys. Acta 511, 125–140.
24 Andrich, M.P. and Vanderkooi, J.M. (1976) Biochemistry 15, 1257–1261.
25 Davenport, L., Dale, R.E., Bisby, R.H. and Cundall, R.B. (1985) Biochemistry 24, 4097–4108.
26 Lesslauer, W., Cain, J.E. and Blasie, J.K. (1972) Proc. Natl. Acad. Sci. USA 69, 1499–1503.
27 Colley, C.M. and Metcalfe, J.C. (1972) FEBS Lett. 24, 241–246.
28 Podo, F. and Blasie, J.K. (1977) Proc. Natl. Acad. Sci. USA 74, 1032–1036.
29 Gulik-Krzywicky, T., Shechter, E., Iwatsubo, M., Ranck, J.L. and Luzzati, V. (1970) Biochim. Biophys. Acta 219, 1–10.
30 Eling, T.E. and Di Augustine, R.P. (1971) Biochem. J. 123, 539–549.
31 Slavik, J. (1982) Biochim. Biophys. Acta 694, 1–25.
32 Holowka, D. and Baird, B. (1983) Biochemistry 22, 3466–3474.
33 Haigh, E.A., Thulborn, K.R. and Sawyer, W.H. (1979) Biochemistry 18, 3525–3532.
34 Lakowicz, J.R., Laczko, G., Cherek, H., Gratton, E. and Limkeman, M. (1984) Biophys. J. 46, 463–477.
35 Kalb, E., Paltauf, F. and Hermetter, A. (1989) Biophys. J. 56, 1245–1253.
36 Parker, C.A. and Rees, W.T. (1960) Analyst (London) 85, 587–600.
37 Hubbell, W.L. and McConnell, H.M. (1971) J. Am. Chem. Soc. 93, 314–326.
38 Pope, J.M. and Dubro, D.W. (1986) Biochim. Biophys. Acta 858, 243–253.
39 Komatsu, H. and Rowe, E.S. (1991) Biochemistry 30, 2463–2470.
40 Nambi, P., Rowe, E.S. and McIntosh, T.J. (1988) Biochemistry 27, 9175–9182.

41 Simon, S.A. and McIntosh, T.J. (1984) Biochim. Biophys. Acta 773, 169–172.
42 Rowe, E.S. (1983) Biochemistry 22, 3299–3305.
43 Rowe, E.S. (1985) Biochim. Biophys. Acta 813, 321–330.
44 Parasassi, T., Conti, F., Glaser, M. and Gratton, E. (1984) J. Biol. Chem. 259, 14011–14017.
45 Barrow, D.A. and Lentz, B.R. (1985) Biophys. J. 48, 221–234.
46 Duportail, G. and Weinreb, A. (1983) Biochim. Biophys. Acta 736, 171–177.
47 Shinitzky, M. and Barenholz, Y. (1974) J. Biol. Chem. 249, 2652–2657.
48 Itoh, T. and Kohler, B.E. (1987) J. Phys. Chem. 91, 1760–1764.
49 Lentz, B.R. and Burgess, S.W. (1989) Biophys. J. 56, 723–733.
50 Matayoshi, E.D. and Kleinfeld, A.M. (1981) Biophys. J. 35, 215–235.
51 Lakowicz, J.R. (1983) Principles of Fluorescence Spectroscopy, Chap. 7, Plenum Press, New York.
52 Blatt, E., Sawyer, W.H. and Ghiggino, K.P. (1983) Aust. J. Chem. 36, 1079–1086.
53 Kai, T., Mak, V.H., Potts, R.O. and Guy, R.H. (1990) J. Controlled Release 12, 103–112.
54 Anderson, B.D. and Raykar, P.V. (1989) J. Invest. Dermatol. 93, 280–286.
55 Liu, P. (1989) Ph.D. Dissertation, The University of Utah, Utah.
56 Bronaugh, R.L. and Maibach, H.I. (1989) Percutaneous Absorption, Marcel Dekker, New York.